2023 IEEE International Conference on Robotics and Automation (ICRA 2023)
May 29 - June 2, 2023. London, UK

# Online Learning and Suppression of Vibration in Collaborative Robots with Power Tools

Gokhan Solak and Arash Ajoudani

***Abstract*— Vibration suppression is an important skill for future robots that will collaborate with humans in industrial settings. The vibration through physical interaction is a common problem in such settings, especially in operations involving hand-held vibrating tools. The existing human-robot collaboration (HRC) works addressing this problem mostly focus on the oscillations caused by the human operator, and suppress them by adapting the admittance parameters. This, however, usually results in stiffer robot behavior and contributes to reducing the overall performance of the task, in particular when impedance planning is a requirement. In this work, we focus on the vibration coming from external sources such as power tools and suppress it actively. We learn the vibration using the bandlimited multiple Fourier linear combiner (BMFLC) algorithm and apply it as a feedforward Cartesian force to cancel the vibration. We combine the feedforward force control with variable impedance learning and show that it improves the vibration suppression performance in simulation and real-world experiments. The feedforward approach can suppress the vibration better while keeping a more compliant set of impedance parameters, which is crucial in HRC.**

## I. INTRODUCTION

Advances in HRC allow robots to enter new environments and face new challenges [1]. Future robots will collaborate with humans in complex and heavy industrial settings, such as construction sites [2]. A construction worker has to use vibrating power tools such as drills, grinders, and air chisels which may cause health problems on long-term exposure, notably the hand-arm vibration syndrome [3]. Therefore, employing collaborative robots for these tasks improves not only productivity but also the safety of humans. For this purpose, we study the use of vibrating tools by collaborative robots.

Unlike solitary industrial robots, collaborative robots have to be flexible and environment-aware to ensure the safety of their human partners. Impedance-based control enables a compliant interaction between the robot and its environment, thus it is widely applied in HRC tasks [1]. Furthermore, variable impedance control increases the awareness of the robot, allowing it to adapt to changing conditions [4]. A variable impedance controller can iteratively adapt to external forces or obstacles by learning not only the impedance but also the feedforward force [5] and the position trajectory [6].

Gokhan Solak and Arash Ajoudani are with HRI$^2$ Lab of Italian Institute of Technology (IIT), Genoa, Italy gokhan.solak@iit.it, arash.ajoudani@iit.it.

This work was supported in part by the H2020 CONCERT project, under grant agreement No. 101016007. The authors would like to thank Mattia Leonori, Sebastian Schleisner Hjorth, and Emir Mobedi for their help in this work.

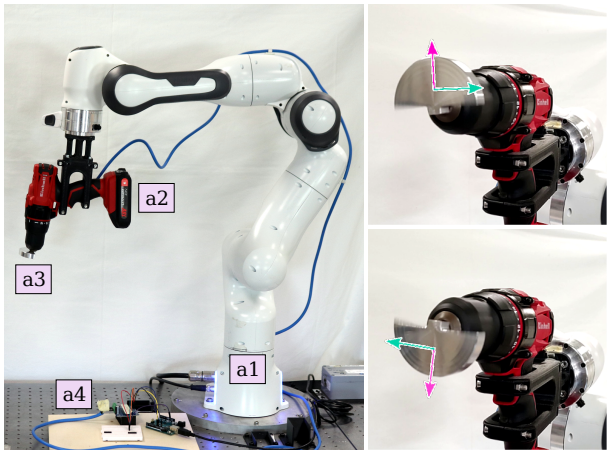


(a) (b)

Fig. 1. (a) We evaluate our method on a 7-DoF Panda robot arm (a1) carrying a modified hand-held drill (a2) with an eccentric drill bit (a3). The rotation speed of the drill is controlled via an Arduino-USB interface (a4). (b) The eccentric mass rotates with the linear velocity shown as the cyan arrow. The rotation creates a centrifugal force illustrated as the magenta arrow. The direction of the centrifugal force alternates periodically, creating a 2D vibration orthogonal to the drilling direction.

Research in collaborative manipulation under arbitrary vibrations focused mainly on the oscillations caused by a human, and prevented the transfer of the oscillating forces to the robot using intermediate mechanisms [7], [8] and variable admittance control [9]. Human-to-robot force-position transfer ratio (admittance) of the interface is regulated either physically, as in [7] using a variable stiffness mechanism; or virtually, as in [9], which observes the vibration level during the interaction and adjusts the control parameters reactively.

Our problem differs as the source of the vibration is a hand-held tool, rather than a human. Therefore, filtering the input of an admittance controller is not an option, as the vibrating tool is attached firmly to the end-effector, causing a direct physical disturbance. In other words, the vibration strength is high enough to perturb the robot motion without an admittance controller to amplify it.

Our empirical studies show that, adjusting only the impedance parameters is not sufficient to cancel powerful vibrations and requires high impedance values to yield an acceptable performance. This however, decreases robot adaptability, which is a crucial requirement for the execution of tasks that need impedance modulation, and may pose risks to collaborating humans.

To address this problem, we first implemented the human-like adaptation (HLA) method [5], an iterative impedance and force learning method which is already shown to cancel

external perturbations such as the addition of an unknown load. However, we observed that this method cannot effectively cancel the vibrating external forces with unknown frequencies. This is because the feedforward force learner cannot distinguish the voluntary motion from the higher-frequency disturbance and it cannot respond to fast-changing forces.

We need a different approach to learn the vibration profile in real-time without perturbing the voluntary motion. Thus, we combine the feedforward force control with variable impedance control. In particular, we adopt the bandlimited multiple Fourier linear combiner (BMFLC) algorithm [10] to learn the vibration signal. This algorithm distinguishes the vibration from voluntary human motion by filtering the error in a target frequency interval. It can learn vibrations consisting of multiple frequency components with varying phase angles, making it suitable for real-world applications.

In summary, we combine iterative variable impedance learning [5] with feedforward vibration cancellation [10] to enable safe and effective collaboration of humans with a robot that uses vibrating tools (Sec. III). We believe this to be a useful skill in industrial settings where robots and humans work side by side, such as at a construction site.

We compared the proposed method to the baseline iterative variable impedance learning method [5] in both simulation and real-robot experiments where the end-effector is continuously perturbed by a vibration source (Sec. IV). The proposed method improves the performance of trajectory tracking by reducing the vibration while allowing a more compliant set of impedance parameters, thus allowing safe human-robot interaction.

We review the related work in the next section and explain our contributions. Then, we present our method (Sec. III), experiments (Sec. IV), and conclusions (Sec. V) in detail.

## II. RELATED WORK

Vibration isolation is studied in various fields to overcome the harmful effects of vibration on machine/structure lifetime [11], control precision [12], and human life quality [13].

Vibration can be suppressed using linear or non-linear physical mechanisms [11]. These mechanisms may adapt to changing conditions by varying their impedance characteristics, e.g., by implementing the stiffness as the distance-dependent magnetic force [7]. However, in this paper, we propose a solution without any task-specific mechanical components, so that our method can be applied using any robotic arm that allows a torque-control interface.

The control-based approaches to vibration suppression use different methods such as variable impedance control [9], [14], input filtering [15], feedback [16] or feedforward control [17], and posture optimization [18]. Our method is novel as we combine variable impedance control and feedforward compensation.

These works do not only differ in their methods but also in the type of vibrations they focus on. The vibrations may happen due to the robot motion control [15], human interaction [9], or external interaction [14]. We focus on the vibration due to external interaction, e.g. using vibrating tools. In this sense, our problem is similar to [14]. However, unlike our work, in [14] the platform is an industrial robot arm that allows very high impedance parameters, and the method involves only parameter adjustment.

In collaborative robotics, vibration suppression was done as an adaptation of the impedance parameters. In this approach, the vibration strength is determined via frequency-domain [19] or time-domain analysis [9] and the impedance is increased to suppress the vibration. Although increasing the damping of the system can decrease the vibration, it also decreases the position accuracy and human-robot interaction transparency. In this work, we show the advantage of feedforward force learning to achieve vibration suppression while keeping the damping parameter low.

There are other applications where a drill is used by a robot, but the vibration aspect of the problem is not on the focus, such as in [20]. Unlike these similar applications, we emulate stronger vibrations using an eccentric mass (Fig. 1) and we focus on the analysis of vibration in our experiments.

Our vibration learning approach is based on the Fourier linear combiner (FLC), which is an adaptive filtering method that models a vibration signal by learning the coefficients of a Fourier series model [21]. However, the original FLC algorithm can only learn vibrations of a previously known single frequency. Consequently, the weighted-frequency FLC (WFLC) was proposed to track vibrations of changing frequency [22], and the BMFLC for modeling vibrations of multiple frequency components in a bandwidth [10]. These were both applied to micro-surgery to cancel the hand tremor of the surgeon using a 1-D actuator [22], [10]. The FLC-derivative algorithms saw many improvements over time, such as [17], which combines WFLC and BMFLC for an adaptive bandwidth. However, for the purposes of this work, the BMFLC was sufficient because it allows learning vibrations of unknown frequencies in a target bandwidth. Using the BMFLC, we show the applicability and benefit of feedforward vibration cancellation in a high-DoF collaborative robot.

Novelties of our work can be summarised as follows:

- We study the feedforward cancellation of tool-sourced vibration for collaborative robots. We experimentally demonstrate the advantage of using feedforward force in comparison to using only impedance adjustment.
- We combine feedforward active vibration cancellation with variable impedance control.
- We apply an FLC-derivative algorithm to cancel vibration in the task-space of a high-DoF robotic arm.

## III. METHODOLOGY

Our control system is built on a Cartesian impedance controller, that transforms the positional errors $(\mathbf{e}_{pos}, \mathbf{e}_{vel})$ into a Cartesian-space force $\mathbf{f}_{imp}$:

$$\mathbf{f}_{imp} = \mathbf{K}_k \mathbf{e}_{pos} \quad + \quad \mathbf{K}_b \mathbf{e}_{vel} \tag{1a}$$

$$\mathbf{e}_{pos} = \mathbf{x}_{des} - \mathbf{x}, \quad \mathbf{e}_{vel} = \dot{\mathbf{x}}_{des} - \dot{\mathbf{x}}. \tag{1b}$$

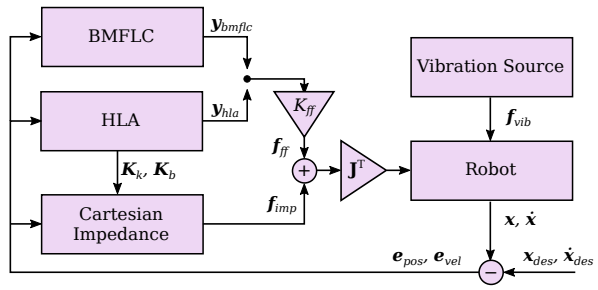


Fig. 2. Our control scheme. The feedforward force $\mathbf{f}_{ff}$ comes from the HLA in the baseline, or from the BMFLC in the proposed method. Gravity and Coriolis compensation, and null-space impedance terms are omitted.

The desired $(\mathbf{x}_{des}, \dot{\mathbf{x}}_{des})$ and actual $(\mathbf{x}, \dot{\mathbf{x}})$ robot poses and twists are represented in 6-D Cartesian-space. The stiffness $\mathbf{K}_k \in \mathrm{R}^{6\times6}$ and damping $\mathbf{K}_b \in \mathrm{R}^{6\times6}$, include linear, rotational, and the coupling terms. We use the boldface style to denote multi-dimensional variables in this report.

On top of our impedance-based controller, we also add the feedforward forces $\mathbf{f}_{ff}$ determined either by the HLA or the BMFLC algorithms to compensate for external perturbations, e.g. vibrations. These forces are added to the impedance control force $\mathbf{f}_{imp}$ and commanded to the robot as the joint torque command $\mathbf{u}$, using the manipulator Jacobian $\mathbf{J}$:

$$\mathbf{u} = \mathbf{J}^\top(\mathbf{f}_{imp} + \mathbf{f}_{ff}). \tag{2a}$$

$$\mathbf{f}_{ff} = \begin{cases} K_{ff}.\mathbf{y}_{hla} & \text{, baseline.} \\ K_{ff}.\mathbf{y}_{bmflc} & \text{, proposed.} \end{cases} \tag{2b}$$

The HLA module also adapts the variable impedance parameters $\mathbf{K}_k$ and $\mathbf{K}_b$ continuously as described below in Sec. III-A.

Fig. 2 illustrates the proposed control scheme. In each of our experiments, there is an external vibration source that generates an oscillating force $\mathbf{f}_{vib}$ to perturb the end-effector's Cartesian position. As shown in the figure, we do not rely on any external force/torque sensors, but only on the robot's proprioception to observe and cancel the perturbations. We also compensate for gravity and Coriolis effects, and apply torques in the null-space of the robot to stay as close as possible to the starting posture, however, these are omitted from the diagram (Fig. 2) for simplicity. In the following sections, we describe how the HLA and BMFLC algorithms work.

### A. Variable impedance control

We implement the HLA method, introduced in [5] as our variable impedance learning method. This method iteratively increases the stiffness $\mathbf{K}_k$, damping $\mathbf{K}_b$, and feedforward term $\mathbf{y}_{hla}$ to minimize the control errors $(\mathbf{e}_{pos}, \mathbf{e}_{vel})$, and slowly returns to a compliant behavior when the errors are low. The terms are updated as follows:

$$\Delta\mathbf{y}_{hla} = \mathbf{Q}_f(\boldsymbol{\varepsilon} - \boldsymbol{\beta}\mathbf{y}_{hla}) \tag{3a}$$

$$\Delta\mathbf{K}_k = \mathbf{Q}_k(|\boldsymbol{\varepsilon}.\mathbf{e}_{pos}^\top| - \boldsymbol{\beta}\mathbf{K}_k) \tag{3b}$$

$$\Delta\mathbf{K}_b = \mathbf{Q}_b(|\boldsymbol{\varepsilon}.\mathbf{e}_{vel}^\top| - \boldsymbol{\beta}\mathbf{K}_b). \tag{3c}$$

The tracking error $\boldsymbol{\varepsilon} = \mathbf{e}_{vel} + \kappa\mathbf{e}_{pos}$, combines the position and velocity errors with a predefined constant $\kappa$. The positive-definite gain matrices $(\mathbf{Q}_f, \mathbf{Q}_k, \mathbf{Q}_b)$ determine the speed of reaction to error. These matrices are determined as a diagonal matrix in the form $\mathbf{Q}_k = Q_k.I$, where $I$ is the identity matrix and $Q_k$ is a scalar. The decay factor $\boldsymbol{\beta}$ recovers the compliance of the system. This term is inversely proportional to the error by a factor of chosen weights $c_1$ and $c_2$, dominating the update value when the error is small:

$$\boldsymbol{\beta} = \frac{c_1}{1 + c_2||\boldsymbol{\varepsilon}||^2}. \tag{4}$$

We use these parameter adaptation terms in the proposed controller as shown in Fig. 2. In this regard, our control of the variable impedance and force is different than [5]. The update rules (3b) and (3c) are slightly different than in [5], as we take the absolute value of the error terms. Otherwise, the error terms could take negative values and decrease the stiffness/damping even though the error magnitudes are getting larger. In addition, we do not learn an interval of values with a known period. This could be useful in a periodic task, however, most tasks do not fall into this category. The vibrations we are trying to learn are of unknown frequencies, thus we use a period of 1 time-step.

### B. Vibration learning

Our system learns the vibration from the velocity error $\mathbf{e}_{vel}$ using the band-limited multiple Fourier linear combiner (BMFLC) algorithm [10]. This algorithm learns the weights $w_k$ of a Fourier series model for each frequency $\nu_r$ in the band:

$$y_{bmflc}(t) = \sum_{r=0}^{L} w_r sin(2\pi\nu_r t) + w_{(r+L)} cos(2\pi\nu_r t). \tag{5}$$

The target frequency band $[\nu_{low}, \nu_{hi})$ is divided into $L$ equally-spaced frequency values $\nu_r$:

$$\nu_r = \nu_{low} + r(|\nu_{hi} - \nu_{low}|/L), \tag{6}$$

with a pair of basis functions $(g_r(t), g_{(r+L)}(t))$ for each frequency component $r \in [1, L)$:

$$g_r(t) = sin(2\pi\nu_r t), \tag{7a}$$

$$g_{(r+L)}(t) = cos(2\pi\nu_r t). \tag{7b}$$

Each weight $w_k$ is updated as follows:

$$\Delta w_k = 2\mu g_k(t) e(t), \quad k \in [1, 2L). \tag{8}$$

The learning rate parameter $\mu$ determines how fast the weights change. Originally, the error term $e(t)$ is defined as the difference between the target value and the BMFLC output $y_{bmflc}(t)$ in [10]. In our system, we use a single-dimensional velocity error $e_{vel}$ directly as $e(t)$. We do not take the difference between $e_{vel}$ and $y_{bmflc}(t)$, because the BMFLC output is already subtracted from the velocity in the form of feedforward control.

We apply the BMFLC on 3D Cartesian-space control. For this purpose, we train an independent Fourier series model (5) for each axis. Consequently, the weight updates (8) use the single dimensional velocity error of that particular axis.

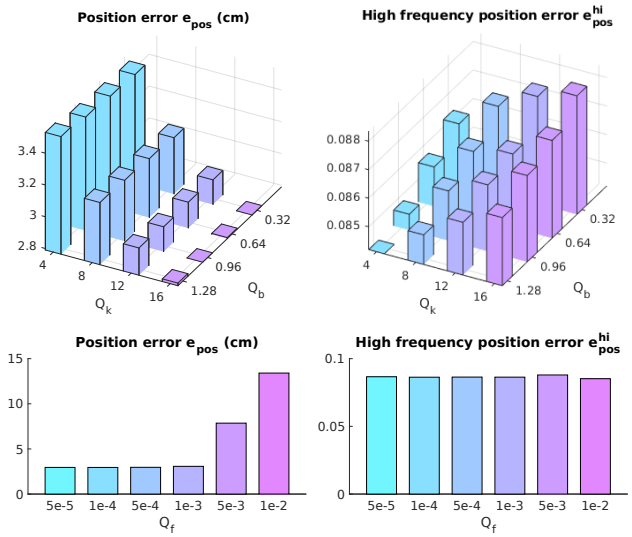


Fig. 3. The MSE results under different HLA impedance learning rates $\mathbf{Q}_k$ and $\mathbf{Q}_b$ (above) and feedforward force learning rates $\mathbf{Q}_f$ (below).

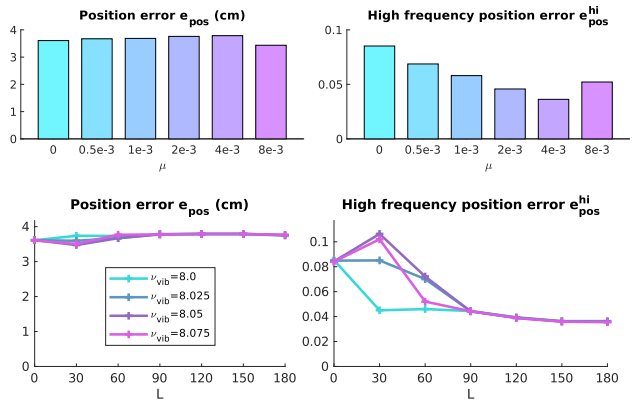


Fig. 4. The effects of the learning rate $\mu$ and the resolution $L$ of the BMFLC. $L$=60 in the $\mu$ experiments, and $\mu$=2 $\times$ $10^{-3}$ in the $L$ experiments. We repeat the $L$ experiments under slightly different vibration frequencies $\nu_{vib}$ to show the importance of resolution.

## IV. EXPERIMENTS

The proposed method is evaluated in simulation and real-world experiments. We first simulate our robot in the Gazebo simulator (*GazeboSim.org*) and test it under a variety of conditions. Then, we carry out real robot manipulation experiments to validate the applicability of our method.

The control scheme (Fig. 2) is common in all of our experiments. The only difference is the vibration generator. In the simulation, we apply continuous sinusoidal force along a single axis of the end-effector frame. In the real robot experiments, we generate the vibrations using a commercial drill with an eccentric drill bit (Fig. 1).

In this work, we study the adaptation of only the translational part of the control. In all of our experiments, the rotational stiffness is set to one-tenth of the initial translational stiffness, and not adapted. The feedforward Cartesian torques along the rotational axes are kept at zero. We also set the desired twist $\dot{\mathbf{x}}_{des}$=0. For most of the experiments, we report $e_{pos}$, the mean squared error (MSE) of $\mathbf{e}_{pos}$ calculated over time, as a measure of control accuracy; and $e^{hi}_{pos}$, the MSE of the high-pass filtered $\mathbf{e}_{pos}$ signal with the cutoff frequency of 3 *Hz*. We use $e^{hi}_{pos}$ to quantify the vibration, i.e. the fast-changing components of the position error.

### A. Simulated robot experiments

We simulate the Franka Emika Panda arm in Gazebo. We created a ROS-Gazebo plugin to continuously apply a sinusoidal force at a chosen link. In our experiments, the plugin applies a single-dimensional force in the *y*-axis of the end-effector. The goal of the robot is to move back and forth 20 *cm* while trying to suppress vibration (>6 *Hz*).

The simulation provides a safe interface to study the effects of various parameters on the system performance. We test the effect of HLA and BMFLC parameters, and the feedforward compensation under different stiffness/damping parameters.

*1) HLA parameters:* This method varies both the impedance w.r.t. $Q_k$ and $Q_b$, and the feedforward force w.r.t. $Q_f$. We aim to test the effectiveness of this method in vibration suppression. The feedforward force comes from the HLA during these experiments.

The decay factor $\beta$ influences all of the update equations (3), and if it is too high, it does not allow the growth of the outputs ($\mathbf{K}_k, \mathbf{K}_b, \mathbf{y}_{hla}$). Thus, we carry out preliminary tests and set the decay constants $c_1$=5 $\times$ $10^{-5}$ and $c_2$=10. Similarly, we set $\kappa$=2, and do not explore these constants further, otherwise, the search space grows too large.

The results (Fig 3) show that the HLA parameters $\mathbf{Q}_k$ and $\mathbf{Q}_b$ create a trade-off between the $e_{pos}$ and $e^{hi}_{pos}$. Increasing $\mathbf{Q}_b$ provides a better vibration compensation, but setting it too high will decrease the control accuracy. We use the parameters of $Q_k$=12, $Q_b$=0.96 in the rest of the experiments.

On the other hand, we did not see any improvement by increasing the feedforward force learning rate $\mathbf{Q}_f$ (Fig 3). Increasing $Q_f$ up to 5 $\times$ $10^{-3}$ breaks the stability of the system, but it is still not sensitive and fast enough to cancel the vibration force. This is because the update rule does not distinguish between the low-frequency and high-frequency components of the error. Since the vibration is generally of a smaller amplitude w.r.t. the trajectory tracking error, it is disregarded. Also, because this term learns from a combination of position and velocity errors ($\boldsymbol{\varepsilon}$) it is affected by the phase shift of the position signal. Thus, we set $Q_f$=0 in the rest of the experiments.

*2) BMFLC parameters:* The learning rate $\mu$ determines the speed of reaction to changes, e.g., when the vibration is introduced or drifted. The system performance does not change for the parameter sets where $\mu K_{ff}$ is the same. Thus we fixed the $K_{ff}$=15 and explored $\mu$ (Fig. 4.a). Too small values of $\mu$ will come short of canceling the vibration, however, too high values of $\mu$ may also decrease the performance because it will change the effective frequency of the output. For instance, if $\mu$ is too high, the BMFLC signal will contain frequencies higher than the bandwidth limit $\nu_{hi}$ that appear due to fast learning.

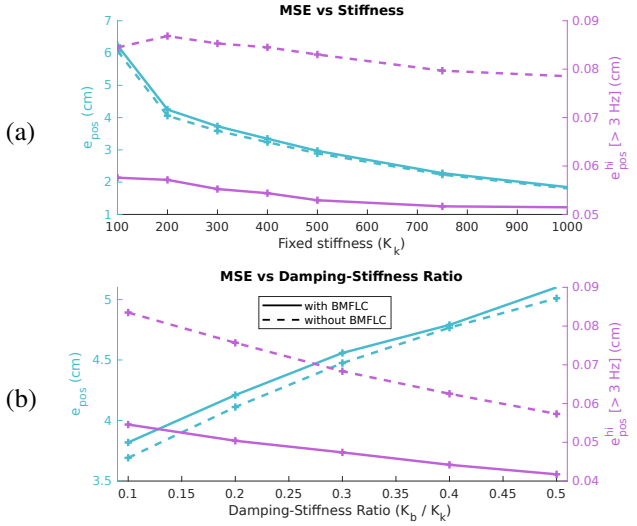


Fig. 5. Effects of increasing (a) the stiffness ($K_k$), and (b) damping/stiffness ratio ($K_b/K_k$) in the simulation experiments. Comparison of the position error $e_{pos}$ (cyan) and high frequency ($>3$ *Hz*) position error $e^{hi}_{pos}$ (magenta), with (solid line) and without (discrete line) feedforward compensation.

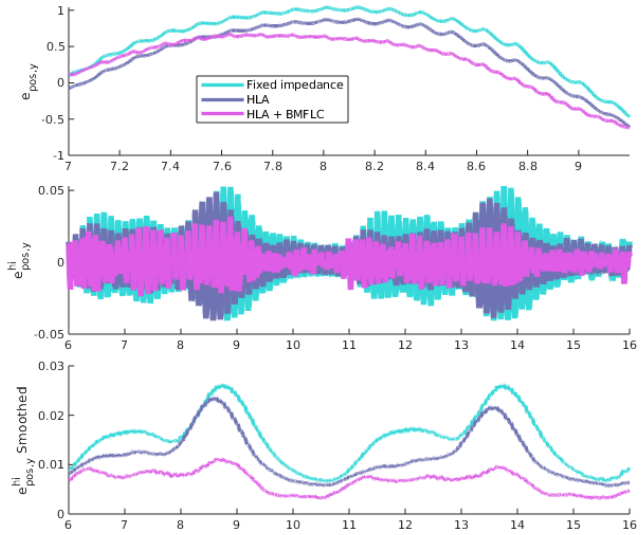


Fig. 6. Comparison of the time series of the position error and its high-frequency components under different methods: (1) Fixed impedance, (2) HLA, and (3) combined HLA and BMFLC. We also show the *smoothed* $e^{hi}_{pos.y}$, where we applied moving average filter on $|e^{hi}_{pos.y}|$. Only a portion of the $y$-axis position is shown for clarity. The vibration is reduced visibly.

The bandwidth is application dependent, we chose it as $[6, 12)$ in this work. It can be adjusted for different needs, however, increasing the bandwidth will increase the computation time or learning error, depending on $L$. For example, choosing $L$=60 means that the bandwidth is divided into 60 points such as $\nu_k = 6.0, 6.1, 6.2, \ldots 11.9$. If the vibration frequency is 6.05, it will not be fully learned. If we increase the bandwidth by twice, then the step size will increase to 0.2, decreasing the accuracy of the learned models.

We experiment with a vibration frequency of 8 *Hz* by default. However, the method can learn for any frequency in the bandwidth, granted that $L$ is high enough. Otherwise, the accuracy may decrease for the drifting values of vibration, such as $8.025, 8.050, 8.075$ which are not included in $\nu_r$ when $L$=60. As the results in Fig. 4 show, the vibration suppression performance decreases for smaller $L$. The accuracy can be maintained by increasing the resolution $L$, however, it means more weight updates for each dimension. Thus, it increases the computation time.

*3) Impedance parameters:* Since the impedance parameters are variable in the HLA method and non-linearly dependent on its parameters ($\mathbf{Q}_k, \mathbf{Q}_b, c_1, c_2$), it is hard to isolate the effect of BMFLC with it.

For a more clear analysis of the feedforward compensation with variable impedance control, we repeat the experiments with varying impedance parameters that are fixed during each trial. We test the effects of both the stiffness and damping parameters on vibration. We first test them under varying stiffness ($K_k \in [100, 200, 300, 400, 500, 750, 1000]$), while keeping the damping factor proportional to stiffness ($K_b$=$1.4\sqrt{K_k}$). Secondly, we test under varying damping/stiffness ratio by increasing the damping ($K_b \in [30, 60, 90, 120, 150]$) while keeping the stiffness constant ($K_k$=300). We execute each case with and without feedforward compensation ($\mathbf{f}_{ff}$).

The effect of stiffness ($K_k$) and damping/stiffness ratio ($K_b/K_k$) on the MSE of position $e_{pos}$ and high-pass filtered position $e^{hi}_{pos}$ are plotted in Fig. 5. The stiffness does not influence the vibration significantly as $e^{hi}_{pos}$ does not change with increased $K_k$. However, we observe that the vibration decreases when the damping to stiffness ratio increases, while the overall error also gets higher as a drawback (Fig. 5.b). The addition of the feedforward force $\mathbf{f}_{ff}$ improves $e^{hi}_{pos}$ significantly, even with low damping. The vibration compensation improves even further if damping is increased together with $\mathbf{f}_{ff}$.

*4) HLA and BMFLC:* We combine these methods for the added value of variable impedance learning in HRC [4] and better vibration suppression. We plot the time series position and high-pass filtered position signals to demonstrate the visible difference between the signals when the same experiment is repeated using fixed impedance, the HLA, and the combination of the HLA and BMFLC (Fig. 6).

### *B. Real robot experiments*

Our real-world robot setup consists of a hand-held drill with an eccentric drill bit mounted on a 7-DoF robot arm (Fig. 1). We control the drill through ROS via an Arduino-USB interface to ensure the same perturbation is applied in repeated experiments. The eccentric rotating mass (ERM) causes 2D sinusoidal vibration with amplitude and frequency depending on the mass, eccentricity, and torque of the ERM. The robot follows a trajectory back and forth between two points in the task space that are *20 cm* apart while suppressing the vibration effects.

Our goal is to validate the applicability of the method in the real world. We first compared a limited set of parameters starting from the optimal parameters of the simulation, and settled on the following parameters: $Q_k$=12, $Q_k$=0.32, $Q_f$=0, $\mu$=0.002, $L$=60, $\nu_{low}$=3, $\nu_{hi}$=9. The ERM causes

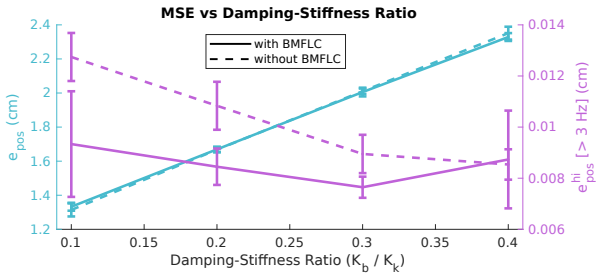


Fig. 7. Effect of increasing the damping/stiffness ratio ($K_b/K_k$) in the real robot experiments. Comparison of the position error $e_{pos}$ (cyan) and high frequency ($>3$ *Hz*) position error $e^{hi}_{pos}$ (magenta), with (solid line) and without (discrete line) feedforward compensation. The plots show the mean and standard deviation of 3 repetitions.

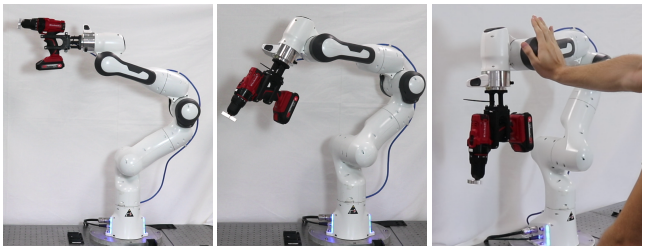

(a) (b) (c)

Fig. 8. The poses looking sideways (a) and diagonally (b), in which we tested our method. The pose looking down is the same as in Fig. 1. (c) Human interaction experiment. The human keeps his extended arm against the robot motion.

vibration with a dominant frequency of $\sim$4.64 *Hz* at the current drill voltage.

*1) Damping-stiffness ratio:* The main experiment of this work is the comparison of vibration cancellation by feedforward force and damping adjustment. In these series of experiments, we apply different damping-stiffness ratios ($K_b/K_k$) from $\frac{1}{10}$ to $\frac{4}{10}$ while keeping the stiffness constant (300); both with and without the feedforward force $\mathbf{f}_{ff}$. The impedance parameters are kept fixed in each trial. Each case is repeated 3 times to observe repeatability.

The results of the damping ratio experiments are presented in Fig. 7. As expected, increasing the damping increases the position error while decreasing the high-frequency components of the error even without the BMFLC. The feedforward compensation further decreases the vibration, even for lower damping ratios. A combination of variable damping and feedforward compensation decreases the vibration some more. However, due to the inaccuracies in the robot model, the vibrations increase for damping ratios larger than $\frac{4}{10}$ for both approaches, unlike the simulation results (Fig. 5).

These results confirm the main findings of the simulation results and validate the benefit of applying feedforward vibration suppression on top of impedance regulation. The feedforward approach can achieve better compensation at lower damping-stiffness ratios, thus allowing the system to maintain its transparency. The suppression can be further improved by also increasing the damping parameter.

*2) Different poses:* We conduct our experiments in the robot pose that is shown in Fig. 1 by default. However, to see the effect of robot kinematics and gravity, we also experiment with different poses as depicted in Fig. 8.

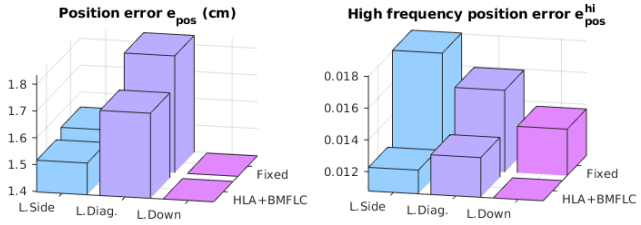


Fig. 9. MSE results of the experiments with different poses.

The experiment is repeated in each pose, with (HLA and BMFLC) and without compensation (Fixed impedance). The outcomes indicate that the vibration compensation is still effective in different postures, decreasing $e^{hi}_{pos}$ (Fig. 9). The new poses cause a larger magnitude of vibration as the 2D vibration generated by the ERM is not orthogonal to gravity anymore. In the pose looking sideways (Fig. 8.a), the vibration axis is parallel to the gravity, thus it adds up to a larger magnitude than the others. However, this also leads to a larger space for improvement, as seen in Fig 9.

*3) Human interaction:* We did a preliminary test of human-robot interaction where a human comes into contact with the robot $\sim$5 *cm* before it reaches the target position, as shown in Fig. 8.c. The proposed method (HLA and BMFLC) actively suppresses the vibration during the entire experiment. The robot measured an 8 *N* force upon contact, as measured through the robot's external torque observer. The contact was maintained for $\sim$5 *s*, in which the stiffness increased by the HLA from 303 to 405 *N/m*, while the applied human force increased up to 15 *N*. In addition to the robot's vibration suppression performance, it maintained a compliant profile, making it suitable for HRC and contact-rich tasks.

## V. CONCLUSIONS

We implemented the vibration cancellation through feedforward force control as part of a variable impedance controller and validated its benefit through simulation and real-world experiments. The feedforward term is learned effectively using the BMFLC, a frequency-dependent zero-phase filtering method. The BMFLC is a more suitable method for learning the feedforward term in the face of fast-changing periodical disturbance, compared to the feedforward term of the baseline method HLA, which is more suitable for slow-changing disturbances such as an added load. The experiments show that feedforward vibration cancellation is more effective in suppressing the vibration than damping adjustment. It can help maintain a higher control accuracy by keeping lower damping values or suppress the vibration further with added damping where desired. The results suggest that the combination of feedforward vibration cancellation with variable impedance learning is a promising framework for future HRC applications.

## REFERENCES


[1] A. Ajoudani, A. M. Zanchettin, S. Ivaldi, A. Albu-Schäffer, K. Kosuge, and O. Khatib, "Progress and prospects of the human-robot collaboration," *Autonomous Robots*, vol. 42, no. 5, pp. 957–975, 2018.

[2] C. Brosque, E. Galbally, O. Khatib, and M. Fischer, "Human-robot collaboration in construction: Opportunities and challenges," in *2020 International Congress on Human-Computer Interaction, Optimization and Robotic Applications (HORA)*. IEEE, 2020, pp. 1–8.

[3] C. Heaver, K. Goonetilleke, H. Ferguson, and S. Shiralkar, "Hand–arm vibration syndrome: a common occupational hazard in industrialized countries," *Journal of Hand Surgery (European Volume)*, vol. 36, no. 5, pp. 354–363, 2011.

[4] F. J. Abu-Dakka and M. Saveriano, "Variable impedance control and learning—a review," *Frontiers in Robotics and AI*, vol. 7, p. 590681, 2020.

[5] C. Yang, G. Ganesh, S. Haddadin, S. Parusel, A. Albu-Schaeffer, and E. Burdet, "Human-like adaptation of force and impedance in stable and unstable interactions," *IEEE transactions on robotics*, vol. 27, no. 5, pp. 918–930, 2011.

[6] Y. Li, G. Ganesh, N. Jarrassé, S. Haddadin, A. Albu-Schaeffer, and E. Burdet, "Force, impedance, and trajectory learning for contact tooling and haptic identification," *IEEE Transactions on Robotics*, vol. 34, no. 5, pp. 1170–1182, 2018.

[7] S. S. Jujjavarapu, A. H. Memar, M. A. Karami, and E. T. Esfahani, "Variable stiffness mechanism for suppressing unintended forces in physical human–robot interaction," *Journal of Mechanisms and Robotics*, vol. 11, no. 2, 2019.

[8] A. S. Ciullo, M. G. Catalano, A. Bicchi, and A. Ajoudani, "A supernumerary soft robotic limb for reducing hand-arm vibration syndromes risks," *Frontiers in Robotics and AI*, p. 227, 2021.

[9] A. Campeau-Lecours, M. Otis, P.-L. Belzile, and C. Gosselin, "A time-domain vibration observer and controller for physical human-robot interaction," *Mechatronics*, vol. 36, pp. 45–53, 2016.

[10] K. C. Veluvolu, U.-X. Tan, W. T. Latt, C. Shee, and W. T. Ang, "Bandlimited multiple fourier linear combiner for real-time tremor compensation," in *2007 29th Annual International Conference of the IEEE Engineering in Medicine and Biology Society*. IEEE, 2007, pp. 2847–2850.

[11] G. Yan, H.-X. Zou, S. Wang, L.-C. Zhao, Z.-Y. Wu, and W.-M. Zhang, "Bio-inspired vibration isolation: Methodology and design," *Applied Mechanics Reviews*, vol. 73, no. 2, 2021.

[12] C. Collette, S. Janssens, and K. Artoos, "Review of active vibration isolation strategies," *Recent patents on Mechanical engineering*, vol. 4, no. 3, pp. 212–219, 2011.

[13] V. Castrillo-Fraile, E. C. Peña, J. M. T. G. y Galán, P. D. Delgado-López, C. Collazo, and E. Cubo, "Tremor control devices for essential tremor: a systematic literature review," *Tremor and Other Hyperkinetic Movements*, vol. 9, 2019.

[14] V. Nguyen, J. Johnson, and S. Melkote, "Active vibration suppression in robotic milling using optimal control," *International Journal of Machine Tools and Manufacture*, vol. 152, p. 103541, 2020.

[15] S. Kumagai, K. Ohishi, and T. Miyazaki, "High performance robot motion control based on zero phase error notch filter and d-pd control," in *2009 IEEE International Conference on Mechatronics*. IEEE, 2009, pp. 1–6.

[16] C. Wang, G. Yang, C.-Y. Chen, Z. Huang, T. Zheng, and S. Chen, "An impedance control scheme with lead-lag controller for flexible joint vibration suppression," in *2017 IEEE International Conference on Cybernetics and Intelligent Systems (CIS) and IEEE Conference on Robotics, Automation and Mechatronics (RAM)*. IEEE, 2017, pp. 742–747.

[17] S. Wang, Y. Gao, J. Zhao, and H. Cai, "Adaptive sliding bandlimited multiple fourier linear combiner for estimation of pathological tremor," *Biomedical Signal Processing and Control*, vol. 10, pp. 260–274, 2014.

[18] H. Girgin, T. S. Lembono, R. Cirligeanu, and S. Calinon, "Optimization of robot configurations for motion planning in industrial riveting," in *2021 20th International Conference on Advanced Robotics (ICAR)*. IEEE, 2021, pp. 247–252.

[19] V. Okunev, T. Nierhoff, and S. Hirche, "Human-preference-based control design: Adaptive robot admittance control for physical human-robot interaction," in *2012 IEEE RO-MAN: The 21st IEEE International Symposium on Robot and Human Interactive Communication*. IEEE, 2012, pp. 443–448.

[20] D. Sirintuna, Y. Aydin, O. Caldiran, O. Tokatli, V. Patoglu, and C. Basdogan, "A variable-fractional order admittance controller for phri," in *2020 IEEE International Conference on Robotics and Automation (ICRA)*. IEEE, 2020, pp. 10 162–10 168.

[21] C. A. Vaz and N. V. Thakor, "Adaptive fourier estimation of time-varying evoked potentials," *IEEE Transactions on Biomedical Engineering*, vol. 36, no. 4, pp. 448–455, 1989.

[22] C. N. Riviere, R. S. Rader, and N. V. Thakor, "Adaptive cancelling of physiological tremor for improved precision in microsurgery," *IEEE Transactions on biomedical engineering*, vol. 45, no. 7, pp. 839–846, 1998.